Electronic structure and crystallographic properties of skutterudite-related $Ce_3M_4Sn_{13}$ and $La_3M_4Sn_{13}$ (M = Co, Ru, and Rh)

A. Ślebarski and J. Goraus
Institute of Physics, University of Silesia, 40-007 Katowice, Poland
(Received 26 July 2013; published 21 October 2013)

The structural and electronic properties of the skutterudite-related $Ce_3M_4Sn_{13}$ and $La_3M_4Sn_{13}$ intermetallic compounds with M = Co, Ru, and Rh have been investigated. A subtle structural transition from a simple cubic phase ($Yb_3Rh_4Sn_{13}$-type structure) to the superlattice variant at $T_D \sim 160$ K has been evidenced by x-ray diffraction, resistivity, and specific-heat data. Recently, a high charge density between metal M and Sn atoms was calculated for $Ce_3Rh_4Sn_{13}$ and $Ce_3Co_4Sn_{13}$. The strong charge accumulation implies a strong M-Sn2 covalent bonding interaction. In consequence, a local distortion of the trigonal Sn prisms around metal M can modify the electronic structure of the system. The main goal of this report is to study the electronic structure in the family of $RE_3M_4Sn_{13}$, where RE = Ce or La above and below T_D. We show that the Sn 4d x-ray photoelectron spectroscopy spectra have the complex structure, which can be interpreted as a result of different charge distribution around Sn atoms. The shape of the 4d Sn lines is also temperature dependent, which we attribute to the local distortion of the Sn2 cages in $RE_3M_4Sn_{13}$.

DOI: 10.1103/PhysRevB.88.155122 PACS number(s): 79.60.−i, 72.15.Qm

I. INTRODUCTION

The ternary compounds $RE_3M_4X_{13}$ (RE is a rare-earth element, M is a transition metal and X is a group-IV element) have attracted considerable attention due to their diverse heavy-fermion properties, also including the interesting interplay of superconductivity and magnetic order, which is closely related to the cage-type structure found in the filled skutterudites. Most of the recent systematic research on these filled cage compounds focused on their thermoelectric properties due to the low phonon thermal conductivities (*rattling* of the rare-earth atoms inside the cage) and the large thermopowers, typical for Kondo systems. Many members of the $RE_3M_4X_{13}$ family crystallize in the simple cubic $Yb_3Rh_4Sn_{13}$ structure ($Pm\bar{3}n$).[1] However, the symmetry of a given parent structure can be lowered by subtle deformation of the X_{12} cages, which can be viewed as a weak superlattice formation of the cubic phase with twice the lattice constant. Such a subtle structural variation can strongly change the band structure at the Fermi level, and in effect the electric transport properties. A recent studies of $Ce_3Co_4Sn_{13}$ revealed;[2,3] e.g., distinct anomalies in the electrical resistivity at $T_D \sim 160$ K, as a result of a local deformation of the $Sn2_{12}$ cages. The observed phase-transition behavior at T_D is similar to charge density wave (CDW) ordering.[4] In this work, we report a detailed investigations of the nature of the transition at T_D in $Ce_3M_4Sn_{13}$ and reference $La_3M_4Sn_{13}$ compounds (M = Ru, Rh, Co) by x-ray diffraction (XRD) and x-ray photoelectron spectroscopy (XPS). We find that the distortion of the $Sn2_{12}$ cages significantly changes the charge distribution of Sn2 atoms and in consequence the charge density accumulation[5,6] between metal M and Sn2 atoms (there is high charge density between Co and Sn2, which implies a strong covalent bonding interaction). We experimentally found that this bonding is similar in the family of $RE_3M_4Sn_{13}$ compounds. In the case of $Ce_3Co_4Sn_{13}$ the hybridization energy Δ_{cf} between the f-electron states and the conduction states, obtained from the Ce 4d XPS spectra, is significantly larger in comparison to the remaining compounds. We argue that the stronger hybridization could be a reason of metal-semimetal transition at T_D in the resistivity data of $Ce_3Co_4Sn_{13}$, not observed for the remaining $Ce_3M_4Sn_{13}$ and $La_3M_4Sn_{13}$ compounds.

II. EXPERIMENTAL DETAILS

Polycrystalline $La_3M_4Sn_{13}$ and $Ce_3M_4Sn_{13}$ samples, where M = Co, Ru, and Rh, have been prepared by arc melting the constituent elements on a water-cooled copper hearth in a high-purity argon atmosphere with an Al getter. The samples were remelted several times to promote homogeneity and annealed at 870 °C for 12 days. Almost no mass loss ($\leqslant 0.02\%$) occurred during the melting and annealing process. All samples were carefully examined by x-ray-diffraction analysis and found to be single phase at room temperature with a cubic structure (space group $Pm\bar{3}n$). The powder-diffraction patterns and the powder-diffraction studies below room temperature were performed using the high-resolution diffractometer Empyreaan (PANalytical B.V.) with the low-temperature camera TTK 450 Anton-Paar.

Stoichiometry and homogeneity were checked by the microprobe technique (scanning microscope JSM-5410) and by XPS analysis, the deviations from the nominal composition were small.

The specific heat C was measured in the temperature range 2–300 K using a Quantum Design PPMS platform. Specific-heat $C(T)$ measurements were carried out on a platelike specimen with a mass of about 10–15 mg utilizing a thermal-relaxation method. The dc magnetization M and the magnetic susceptibility χ results were obtained using a commercial superconducting quantum interference device magnetometer from 1.8 to 300 K.

The XPS spectra were obtained with monochromatized Al K_α radiation at room temperature using a PHI 5700 ESCA spectrometer. The polycrystalline sample was broken under high vacuum better than 6×10^{-10} Torr immediately before taking a spectrum.

The band-structure calculations were accomplished using fully relativistic full potential local orbital (FPLO) method (FPLO9-00-34 computer code[7]) within the local spin density approximation (LSDA). The exchange correlation potential V_{xc} was used in the form proposed by Perdew-Wang.[8] The number of k points in the irreducible wedge of the Brillouin zone was 20 for both $Ce_3Ru_4Sn_{13}$ and $La_3Ru_4Sn_{13}$ systems; due to a large volume of the unit cell this number was found sufficient to obtain well converged results. The spin-orbit interactions considered within fully relativistic calculations reduce the symmetry of the magnetic unit cell depending on the chosen magnetization axis. In our calculations we used (0,0,1) as the chosen direction of the magnetization axis. For a comparison of experimental Sn 4d XPS spectra with the calculated one we used the following procedure: calculated density of states (DOS) were multiplied by a proper cross section taken from Ref. 9, and convoluted by the Lorentzian line with a full width at half maximum (FWHM) of 0.4 eV to account for the instrumental resolution and the effect of the lifetime of the hole states.

III. RESULTS AND DISCUSSION

A. Structure

Room-temperature XRD on $Ce_3M_4Sn_{13}$ and $La_3Co_4Sn_{13}$, where M = Co, Ru, and Rh confirms the cubic structure of the $Yb_3Rh_4Sn_{13}$ type (cf. Fig. 1). The XRD data for $Ce_3Co_4Sn_{13}$ do not indicate any structural change at the lower temperatures, whereas the XRD diffraction patterns obtained for the remaining compounds at $T = 85$ K show additional weak superlattice reflections in the low 2θ region, indicating a lower symmetry of cubic structure with a lattice parameter twice that of the high-temperature phase. The transformation into the weakly distorted phase [cf. the inset to Figs. 1(a) and 1(b)] is detected at the same temperature T_D, where distinct anomalies are observed in the resistivity,[3] specific-heat, and susceptibility data (as will be discussed). Figure 2 shows the temperature dependencies of the distance $d(T)$ normalized to the d value at $T = 300$ K between (622) crystallographic planes, obtained from the Bragg equation $\lambda = 2d\sin\theta(T)$ for diffraction line (622). In Fig. 3 the intensity of the (622), (542), and (631) Bragg reflections exhibits small change at T_D, which again can be explained by the local distortion of the cages. The effect is due to the slight movement of Sn2 atoms: in the initial structures, only the Sn2 atoms are not located at the most stable position. These superlattice reflections have been very faint, less than 1% of the maximum intensity of the parent lattices, therefore similar superlattice transition can be overlooked in the XRD low-temperature data for $Ce_3Co_4Sn_{13}$. The atomic positions and structural information, which were obtained from the full x-ray-diffraction patterns are summarized in Table I. The structures at $T = 300$ and 85 K were solved by Rietveld analysis and refined using the FULPROF package.[10] By comparing the Sn2 positions (and interatomic distances Sn1-Sn2, RE-Sn2, and M-Sn2), we observe that the distances $Sn1(Sn2)_{12}$, $RE(Sn2)_4$, and $RE(Sn2)_8$ are evidently temperature dependent, which suggests that the low-T structure is locally distorted.

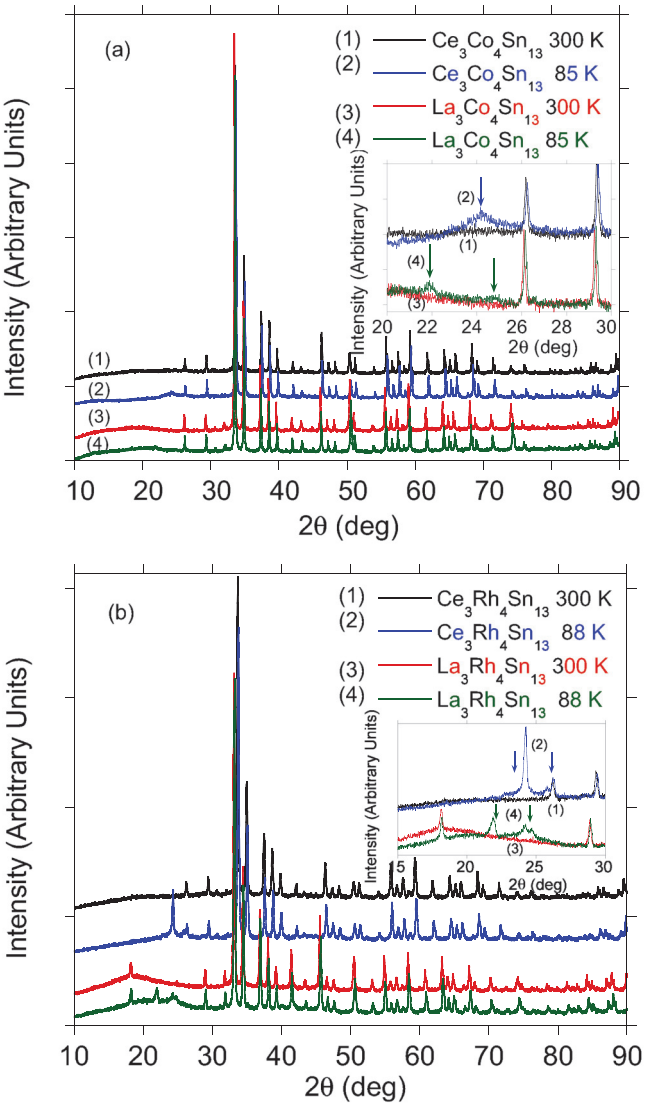

FIG. 1. (Color online) X-ray diffraction (XRD) of $Ce_3Co_4Sn_{13}$ and $La_3Co_4Sn_{13}$, (a) and $Ce_3Rh_4Sn_{13}$ and $La_3Rh_4Sn_{13}$ (b) with Cu K_α radiation at 300 and 85 K. The inset presents the XRD patterns for small 2θs to exhibit additional superlattice reflections.

B. Electronic structure obtained from the XPS spectra

Figures 4(a)–4(c) display the valence-band (VB) XPS spectra for $Ce_3M_4Sn_{13}$, with M = Co, Ru, and Rh, and the La counterparts, measured at room temperature and at $T = 130$ K, respectively. The related spectra measured at two different temperatures are almost identical and do not exhibit any significant change of shape below and above the temperature T_D. The most intense peak in valence-band spectra originates mainly from the metal M d states hybridized with 5p states of Sn.[5,6] The second peak centered at ~7 eV is related to photoemission from Sn 5s states. Direct comparison of the $Ce_3M_4Sn_{13}$ and $La_3M_4Sn_{13}$ VB XPS spectra shows in Figs. 4(a)–4(c) that there is no difference in their shape, which means that the Ce 4f states give only a small contribution to the measured spectrum. The nearest-neighbor Ce-Ce distance of ~4.7 Å is large, which leads to formation of narrow 4f bands with their negligible contribution to the chemical bonding

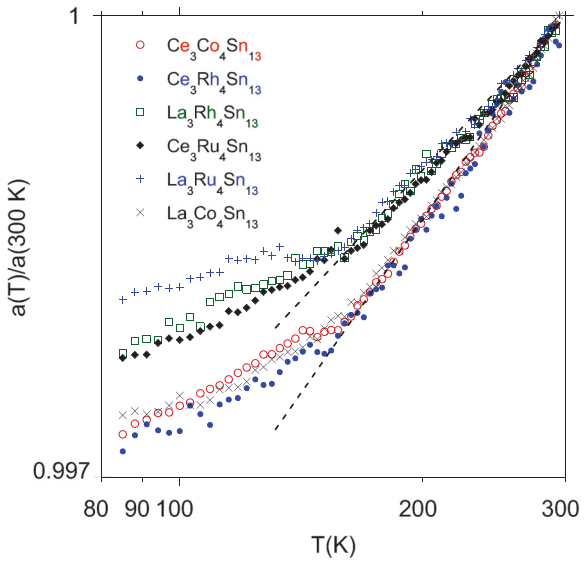

FIG. 2. (Color online) The temperature change of $d_{622}(T)$ for the (622) XRD line between 85 and 300 K, and normalized to d_{622} value at $T = 300$ K in log-log scale.

as has been calculated (cf., Refs. 5 and 6). The interaction between Ce and M as well as Sn atoms is realized by the coupling of $4f$ and conduction-electron states. Analysis of the Ce $3d$ core-level XPS spectra is an efficient tool for obtaining experimentally the character of the $4f$ states owning to the strong Coulomb interaction between the photoemission core hole and the electrons located at the Fermi level. For a Kondo lattice state, the ground state of a Ce- and La-based compound is very sensitive to both the magnitude of the hybridization energy Δ_{cf}, and the occupancy of the f shell, n_f.[11] Energy Δ_{cf}, which describes the hybridization part of the Anderson impurity Hamiltonian,[11] is defined as $\pi V^2 N(\epsilon_F)$, where $N(\epsilon_F)$ is the density of states (DOS) at the Fermi level ϵ_F, and V is the hybridization matrix element. The microscopic parameters of the Anderson-lattice model, V and n_f, can be determined experimentally from the Ce $3d$ XPS

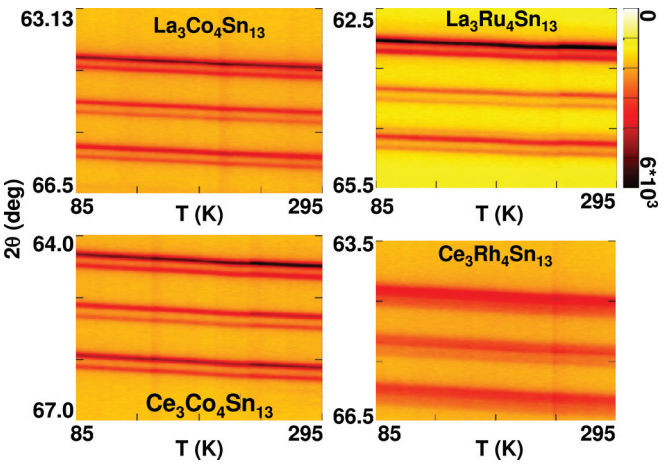

FIG. 3. (Color online) Temperature dependence of the intensity and $2\theta_B$ Bragg reflection's maxima of the diffraction lines (622), (542), and (631). There is a change of intensity at $T_D \sim 160$, T_D also separates two slopes in $2\theta(T)$ vs T plots.

TABLE I. $RE_3M_4Sn_{13}$, RE = Ce, La, M = Co, Ru, Rh; lattice parameters a (in Å) and the atomic positions of Sn2 (Wyckoff site $24k$) at $T = 300$ and 85 K, obtained from the Rietveld analysis.

			Coordinates of Sn2 atom		
Compound	T (K)	a (Å)	x	y	z
$Ce_3Co_4Sn_{13}$	300	9.5881(5)	0	0.2987(6)	0.1482(4)
	85	9.5680(1)	0	0.3008(9)	0.1438(6)
$La_3Co_4Sn_{13}$	300	9.6312(5)	0	0.3034(6)	0.1504(0)
	85	9.6153(7)	0	0.3066(0)	0.1468(2)
$Ce_3Ru_4Sn_{13}$	300	9.7217(8)	0	0.2992(9)	0.1441(0)
	85	9.7004(8)	0	0.2904(0)	0.1544(0)
$La_3Ru_4Sn_{13}$	300	9.7665(8)	0	0.3091(9)	0.1541(6)
	85	9.7473(0)	0	0.3111(6)	0.1541(6)
$Ce_3Rh_4Sn_{13}$	300	9.5920(0)	0	0.3009(4)	0.1438(6)
	85	9.5671(9)	0	0.2904(6)	0.1543(9)
$La_3Rh_4Sn_{13}$	300	9.7408(8)	0	0.3082(3)	0.1541(6)
	85	9.7400(0)	0	0.3078(7)	0.1541(6)

spectra using the Gunnarsson-Schönhammer (GS) theory.[12] In Fig. 5, we plot the deconvoluted Ce $3d$ core-level XPS spectra for $Ce_3Co_4Sn_{13}$ (a), $Ce_3Ru_4Sn_{13}$ (b), and $Ce_3Rh_4Sn_{13}$ (c) at room temperature and at $T = 130$ K, respectively. For comparison, we also present the La $3d$ XPS spectra (Fig. 6) obtained for reference compounds. The separation of the overlapping peaks in the XPS spectra was carried out on the basis of the Doniach-Šunjić interpretation scheme.[13] The main components $3d^9_{5/2}4f^1$ and $3d^9_{3/2}4f^1$ exhibit a spin-orbit splitting of magnitude $\Delta_{SO} = 18.6$ eV. The presence of the $3d^94f^2$ components is a clear manifestation of the intraatomic hybridization between the $4f$ electrons and conduction band. From the analysis of these spectra (for details on the procedure see also Ref. 14), one obtains the hybridization energy Δ_{cf} from the intensity ratio $I(f^1)/[I(f^2) + I(f^1)]$ with the accuracy of the order of 20%, listed in Table II. Within the approximations inherent in the GS theory some error in determination of Δ_{cf} is due to the uncertainty in the intensity ratio $3d^9f^1 : 3d^9f^2$, directly related to the accuracy of the decomposition of the spectrum, as well as due to a proper background subtraction.[14] The high-energy $3d^9f^0$ components of the $3d$ XPS spectra, roughly $\sim$11 eV away from the $3d^94f^1$ peaks, are expected for Ce^{4+} configuration[12] in the case of mixed or valence fluctuated Ce-based compounds; this is, however, not the case for the family of $Ce_3M_4Sn_{13}$. In Fig. 5 the spectra obtained below and above T_D are very similar. One can therefore deduce that the f-electron shell of Ce^{3+} ions is stable, and the hybridization between $4f$ electrons and the conduction states (cf. Table II) is rather small, and temperature independent. It also means that the effect of f-conduction-band hybridization is not a cause for distortion and associated abnormalities at $T = T_D$. There is additional evidence for Ce^{3+} in $Ce_3M_4Sn_{13}$, displayed in Fig. 7. The Ce $4d$ XPS spectra do not show satellite peaks at binding energies of $\sim$118–124 eV, which could be attributed to $3d^94f^0$ cerium final states (for details, see Refs. 15 and 16). The Ce and La $4d$ XPS spectra are not temperature dependent, which again supports the stable configuration of Ce ions.

The bonding length of transition metal M and Sn2 is $\sim$2.6 Å, much shorter than the distance Ce-Sn2 ($\sim$3.4 Å) which

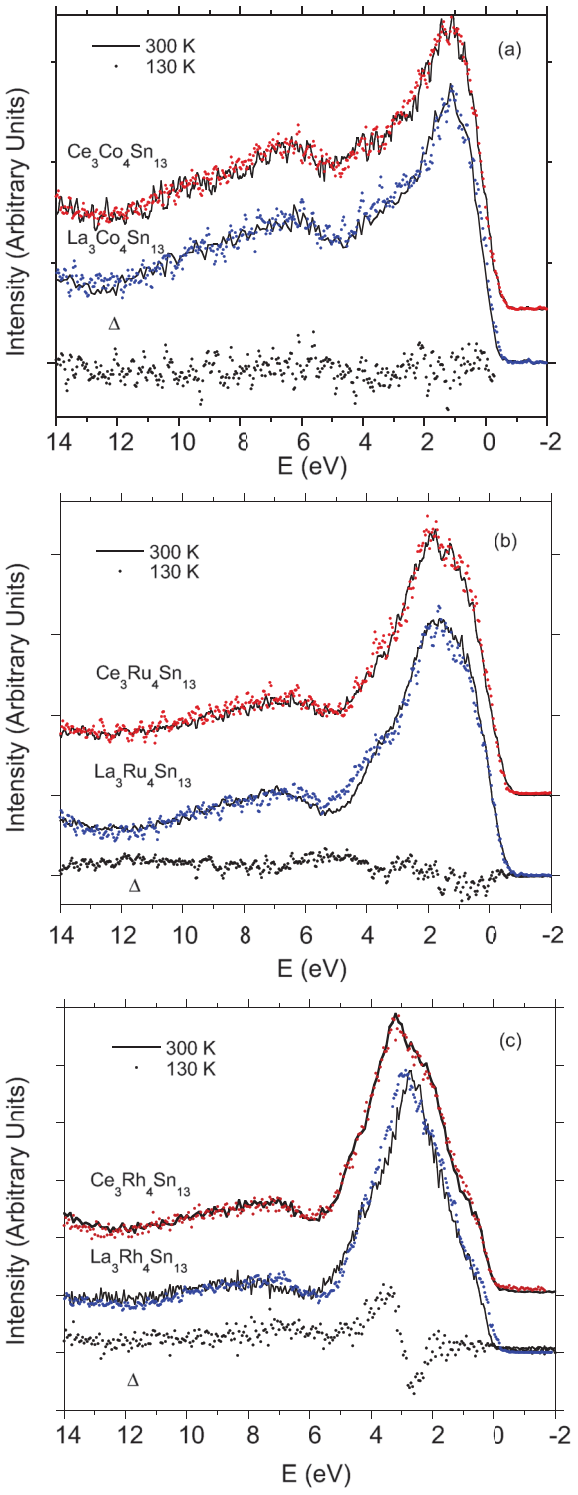

FIG. 4. (Color online) Valence-band XPS spectra measured at room temperature and at 130 K for $Ce_3Co_4Sn_{13}$ and $La_3Co_4Sn_{13}$ (a); $Ce_3Ru_4Sn_{13}$ and $La_3Ru_4Sn_{13}$ (b), and $Ce_3Rh_4Sn_{13}$ and $La_3Rh_4Sn_{13}$ (c), respectively. Δ is the difference at $T = 300$ K between the VB XPS spectra of $Ce_3M_4Sn_{13}$ and respective La references.

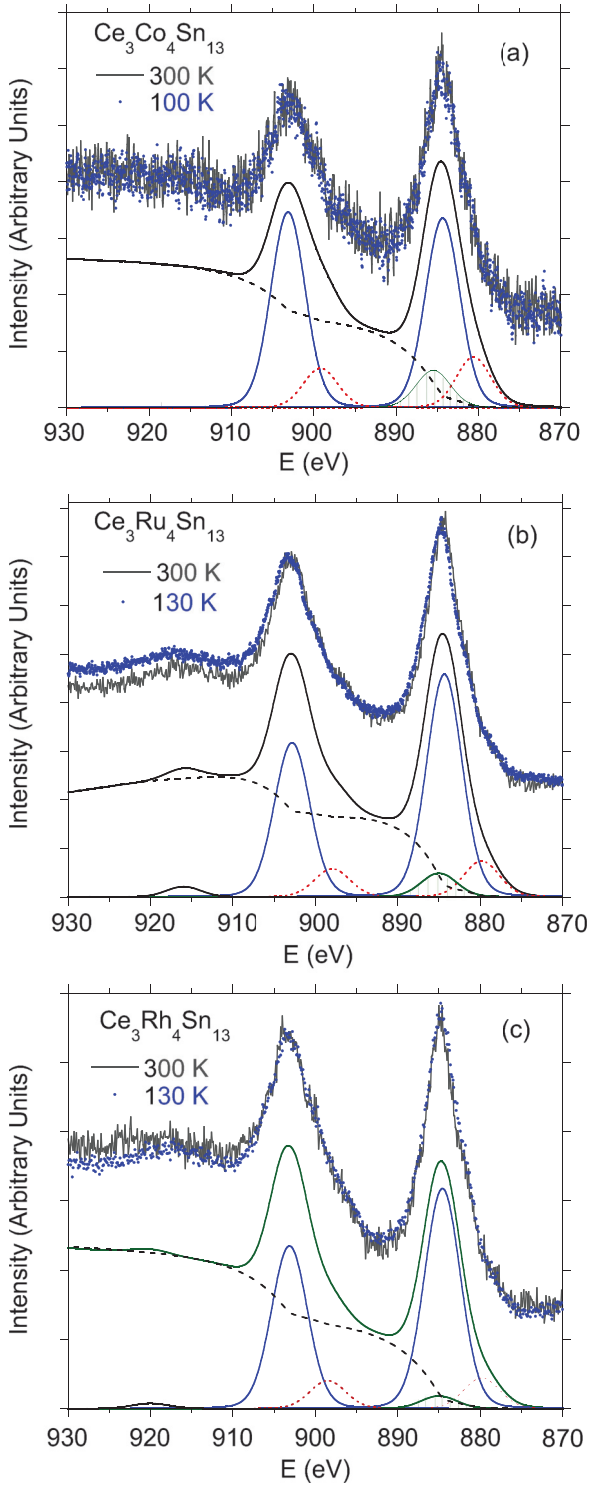

FIG. 5. (Color online) The Ce 3*d* XPS spectrum for $Ce_3Co_4Sn_{13}$ (a), $Ce_3Ru_4Sn_{13}$ (b), and $Ce_3Rh_4Sn_{13}$ (c) deconvoluted based on the Gunnarsson and Schönhammer theoretical model. The Sn 3*s* peak at 885 eV (the line area filled with bars) provides ∼15% of the total peak intensity due to $3d^9_{5/2}4f^1$ final states.

suggests the hybridization states due to strong interaction among Co and Sn valence-band electronic states. Indeed, the difference charge density analysis[5,6] displays charge accumulations between metal *M* and Sn2 atoms, which implies a strong covalent bonding interaction. The second type of charge accumulations indicate multicenter bonds between the Sn2 atoms with possible contribution from the surrounding Ce atoms and one Sn1 atom; the effect is, however, much

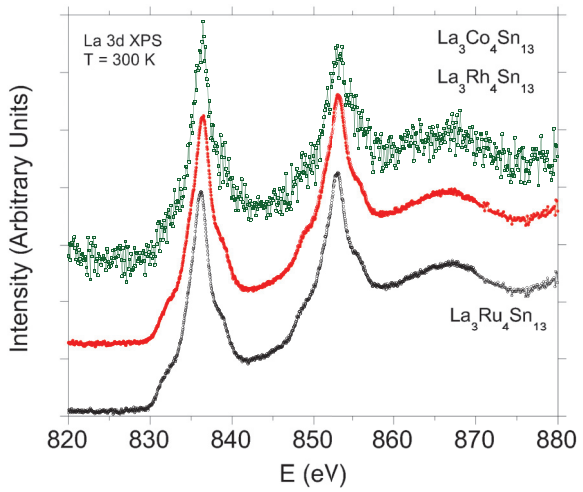

FIG. 6. (Color online) The La 3*d* XPS spectra for $La_3Co_4Sn_{13}$, $La_3Ru_4Sn_{13}$, and $La_3Rh_4Sn_{13}$ at room temperature.

weaker. A very recent observation of a possible charge density wave ordering[4] in $Ce_3Co_4Sn_{13}$ below T_D has also provided microscopic evidence for a change of electronic states in Sn2 due to the slight movement and/or distortion of the Sn2 atom from its initial position. For this reason we investigate the Sn 4*d* XPS spectra which should include the change of local symmetry in the Sn sites above and below temperature T_D in the shape of the Sn 4*d* line. In Fig. 8 are shown the Sn 4*d* core-level spectra for $Ce_3M_4Sn_{13}$ (a) and $La_3M_4Sn_{13}$ (b). They consist of two peaks at 24 and ∼25 eV binding energy with a spin-orbit splitting of ∼1 eV and a smaller broad feature between 26 and 28 eV, located on the high-energy side of the line. We note that (i) the intensities of the 5/2 and 3/2 peaks are not in proportion 3:2, and (ii) the intensity ratio $d_{5/2} : d_{3/2}$ and the shape of the broad feature is temperature dependent. This can be explained as follows: (i) The effect is caused by Sn atoms with two different valencies (e.g., the case for $SnTaS_2$; Ref. 17). This scenario, however, does not explain the presence of the high-energy side broad feature in the 4*d* Sn line. Second, (ii) the surface content of oxygen could modify the spectra; in this case there is usually observed one broad line at the binding energy ∼27 eV.[18] Assuming that the shape of the 4*d*

TABLE II. Hybridization parameter Δ obtained from GS analysis of the Ce 3*d* XPS spectra at 300 and 130 K.

Compound	T (K)	Δ (meV)
$Ce_3Co_4Sn_{13}$	300	140 ± 30
	130	121 ± 25
$La_3Co_4Sn_{13}$	300	80 ± 16
	130	75 ± 16
$Ce_3Ru_4Sn_{13}$	300	70 ± 15
	130	95 ± 15
$La_3Ru_4Sn_{13}$	300	73 ± 15
	130	65 ± 14
$Ce_3Rh_4Sn_{13}$	300	55 ± 12
	130	55 ± 12
$La_3Rh_4Sn_{13}$	300	73 ± 15
	130	90 ± 20

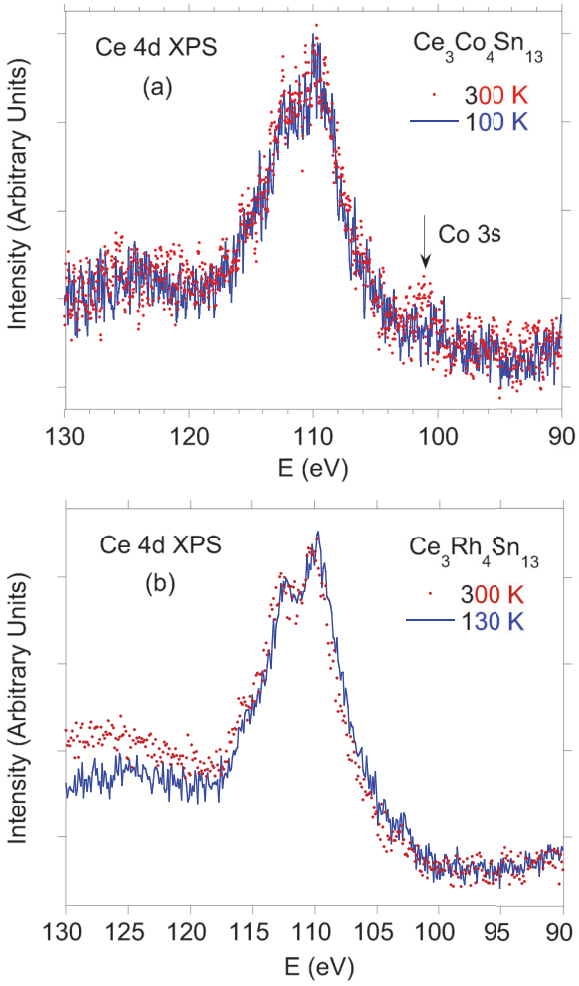

FIG. 7. (Color online) The Ce 4*d* XPS spectra of $Ce_3Co_4Sn_{13}$ (a) and $Ce_3Rh_4Sn_{13}$ (b) measured at $T = 300$ and 130 K, with no evidence of the $4d^9 4f^0$ components.

Sn line corresponds to the oxygen surface content, one also can expect oxygen contribution to the shape of the Ce and La 3*d* and 4*d* XPS spectra, which are very sensitive on the oxygen content too, whereas in Figs. 5–7 the spectra do not exhibit any oxygen contribution. The spectra were measured after breaking the sample in the vacuum better than 6×10^{-6} Torr, and the overview XPS spectra display only a very small amount of oxygen after experiment. We suggest an explanation of the abnormal shape of the Sn 4*d* line on the base of change of local symmetry of the Sn2 icosahedra. First, we have shown how the symmetry determines the electronic structure of Sn. In Fig. 9 we present the Sn 4*d* DOS calculated for three different symmetries within the Sn site using the fully relativistic FPLO method. We consider elemental Sn crystallizing within tetragonal $I41/amd$ space group, as well as $CeSn_3$ and Ce_3Sn both crystallizing within $Pm3m$ space group, but with Sn atoms located at different Wyckoff positions. In $CeSn_3$ Sn occupies 3*c* Wyckoff sites, while in Ce_3Sn Sn is located in the Wyckoff position 1*a*. Figure 9 shows that the shape of the 4*d* Sn DOS is dramatically different in each of the cases. The 4*d* states in elemental Sn are shallow and very broad, whereas the 4*d* states in $CeSn_3$ and Ce_3Sn are very narrow and well localized. The localization of

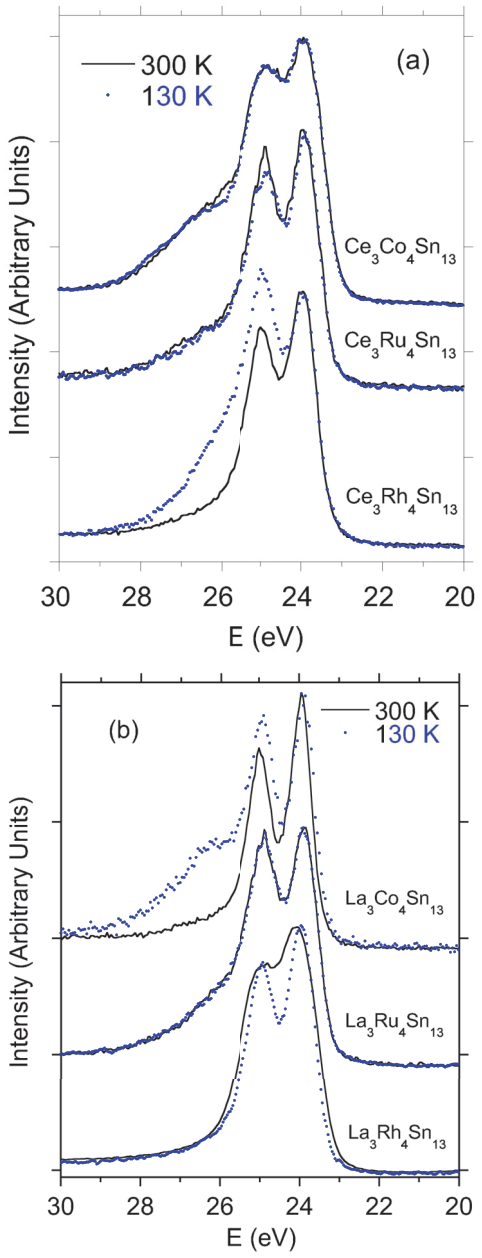

FIG. 8. (Color online) the comparison of the Sn 4*d* XPS spectra obtained at $T = 300$ and 130 K for $Ce_3M_4Sn_{13}$ (a) and for $La_3M_4Sn_{13}$ (b) $M =$ Co, Ru, or Rh.

the 4*d* Sn states is caused by the charge transfer. Based on the Mulliken population analysis[19] Sn donates 0.21 electrons in $CeSn_3$, 0.84 electrons in Ce_3Sn, while in elemental Sn the electron transfer is by definition equal to 0. When the spin-orbit coupling is taken into consideration, the Sn sites in $CeSn_3$ exhibit lower than cubic symmetry, which is reflected in a visible split of the 4*d* Sn line in this compound. In a similar way we also can study the change of local symmetry and the charge transfer in the Sn site for the more complicated systems caused by doping or temperature. In Fig. 10 we compare the calculated shape of the Sn 4*d* line of $Ce_3Ru_4Sn_{13}$ and $La_3Ru_4Sn_{13}$, convoluted with Gaussian 0.4 eV. The calculated

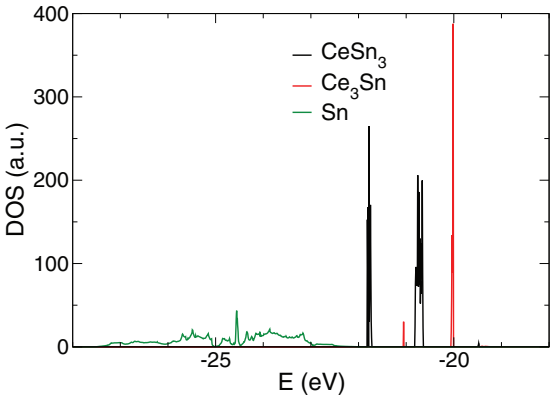

FIG. 9. (Color online) The Sn 4*d* DOS in fully relativistic FPLO method calculated for elemental Sn (symmetry $I41/amd$), $CeSn_3$ ($Pm3m$, Sn in 3*c* sites), and Ce_3Sn ($Pm3m$, Sn occupies the 1*a* sites). The shape of the 4*d* Sn states is quite different in each case. DOS is plotted in arbitrary units (a.u.).

ratio of the intensity of two split Sn 4*d* lines is different for both compounds, also the linewidths are slightly different.

Based on these calculations, we argue that the 4*d* Sn XPS lines shown in Fig. 8 should give evidence of the real electronic state of Sn in the samples $La_3M_4Sn_{13}$ and $Ce_3M_4Sn_{13}$. The complex structure of the Sn 4*d* XPS lines confirms the charge accumulation around Sn2 atoms, obtained from the calculated difference charge density[5,6] either for $Ce_3Rh_4Sn_{13}$ or $Ce_3Co_4Sn_{13}$. XPS measurement carried out at various temperatures also shows a change in the shape of the 4*d* spectra; this behavior may result from the structural local distortion of the $(Sn2)_{12}$ icosahedra at the temperature $T_D \sim 160$ K.

C. The consequences of the crystal structure distortion on thermodynamic properties of $Ce_3M_4Sn_{13}$ and the $La_3M_4Sn_{13}$ counterparts; some new remarks

The key message of this work is to explain the anomaly in the temperature dependence of lattice parameters, specific heat, magnetic susceptibility, and resistivity (the resistivity is not shown in this work) of the $Ce_3M_4Sn_{13}$ and $La_3M_4Sn_{13}$ compounds which may be caused by a subtle structural transition from the simple cubic structure at room temperature

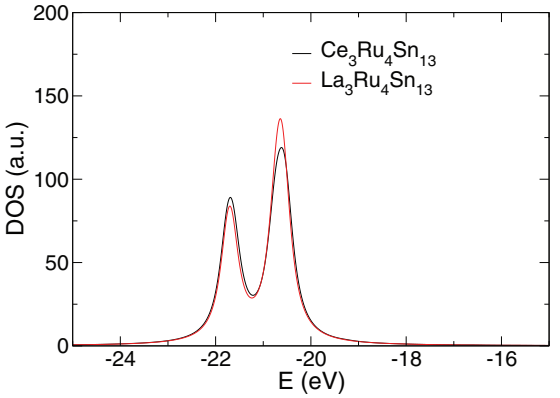

FIG. 10. (Color online) The calculated 4*d* Sn XPS spectra for $Ce_3Ru_4Sn_{13}$ and $La_3Ru_4Sn_{13}$; the 4*d* DOSs were convoluted with Gaussian 0.4 eV. DOS is plotted in arbitrary units (a.u.).

to a superlattice variant close to 160 K. Referring to our earlier report[3] there is a a connection between charge accumulation in the bonding of nearest-neighboring Sn2 and M atoms,[5,6] leading to a local distortion in the M atom environment which then modifies the electronic structure, and diverse physical properties of these compounds. A similar view was very recently presented for $Ce_3Co_4Sn_{13}$ (Ref. 4) and $(Sr/Ca)_3Ir_4Sn_{13}$,[20] where the formation of a charge density wave (CDW) state or a novel superlattice quantum critical point, respectively, may arise below T_D as a result of a superlattice transition. In both cases the electrical resistivity, specific heat, and magnetic susceptibility exhibit significant and qualitatively similar anomalies at T_D. However, an attempt to explain the anomalies based on the subtle structural deformation of the bonding between the Sn2 and M atoms differs fundamentally from the interpretation proposed by Thomas *et al.*,[2] who attributed the abnormal shoulder in the $\rho(T)$ data of $La_3Co_4Sn_{13}$ between 10 and 160 K to the s-d scattering between the conduction electrons from the unfilled Co d band, i.e., not related to a structural anomaly. From the literature we know several Sn-based ternary phases with La and transition-metal M where the s-d scattering contribution[21] to electron-phonon scattering well approximates the electrical resistivity in the wide temperature region, e.g., the series of LaMSn intermetallic compounds.[22] In the case of $Ce_3Co_4Sn_{13}$ the interband scattering processes seems to be supported by a single-crystal x-ray-diffraction experiment at 140 K which shows no change in the crystal structure from that of the room-temperature data. Our recent x-ray-diffraction experiment[3] on the polycrystalline sample of $Ce_3Co_4Sn_{13}$ also did not give evidence for structural change at ∼160 K, however, the intensity of the Bragg reflections exhibited a significant change at T_D, which was explained by the local distortion of the cages. It seems likely that the superlattice reflections could be too weak to be detected. In contrast, the remaining compounds clearly show additional weak superlattice reflections in the low 2θ region (cf. Fig. 1), indicating a lower symmetry of cubic structure with a lattice parameter twice that of the high-temperature phase.

To argue the interpretation that electronically driven superlattice distortion first of all leads to the anomalies of the physical quantities near T_D, first (i) we discuss the susceptibility data displayed in Fig. 11. The zero-field-cooling (ZFC) and FC susceptibilities of $La_3Co_4Sn_{13}$ and $La_3Ru_4Sn_{13}$ show a weak feature at ∼130 K and significant divergence at the lower temperatures. A similar weak feature was also observed in the $\chi(T)$ data for $La_3Rh_4Sn_{13}$ at at similar temperature (not shown in the figure), however, the divergence in the ZFC and FC data is negligible. The spin fluctuations in $La_3M_4Sn_{13}$ can be a possible origin of these low-temperature anomalies in $\chi(T)$. Former calculations within local spin density (LSDA + U) approximation[4,5] obtained $La_3Rh_4Sn_{13}$ and $La_3Co_4Sn_{13}$ nonmagnetic, however, since there is a significant contribution of metal M = Rh or Co states to the Fermi surface, the nesting instabilities might be the origin for the observed anomalies. Note that the calculated ground state of $La_3M_4Sn_{13}$ is nonmagnetic, however, the difference of total energies of the nonspin-polarized and spin-polarized ground states is less than 1 meV, therefore a strong magnetic instability is possible. It has been shown too that a slight movement of the Sn2 atom from its initial position significantly changes the electronic states

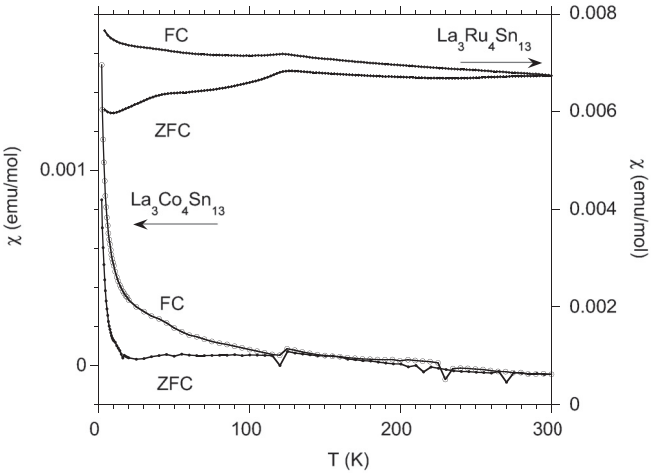

FIG. 11. Magnetic susceptibility (dc) for $La_3Co_4Sn_{13}$ and $La_3Ru_4Sn_{13}$ in external magnetic field of 0.1 T measured in options: zero field cooling (ZFC) and field cooling (FC).

giving rise to magnetic instabilities.[5] The calculations give the high charge density between Sn and M and similar Fermi surface in $La_3M_4Sn_{13}$ and $Ce_3M_4Sn_{13}$, therefore the ZFC and FC effect in the susceptibility should also be observed in the Ce compounds; this is, however, not the case. As shown in Fig. 11 the maximal ZFC and FC divergence in χ of $La_3M_4Sn_{13}$ is very small and less than 0.5% of the magnetic susceptibility at 2 K of $Ce_3M_4Sn_{13}$ counterparts; this is a possible explanation while a very weak effect due to the d-electron states of metal M is not measured (we only note a very small divergence below ∼7 K between ZFC and FC magnetic susceptibility which is about 3% of ZFC χ at $T = 2$ K for $Ce_3Co_4Sn_{13}$, about 1% for $Ce_3Ru_4Sn_{13}$, whereas the effect is negligible in $Ce_3Rh_4Sn_{13}$). (ii) The specific-heat data displayed in Fig. 12 show that the observed anomalies in $C(T)$ are not typical of a classical structural phase transition. The inset shows a derivative of

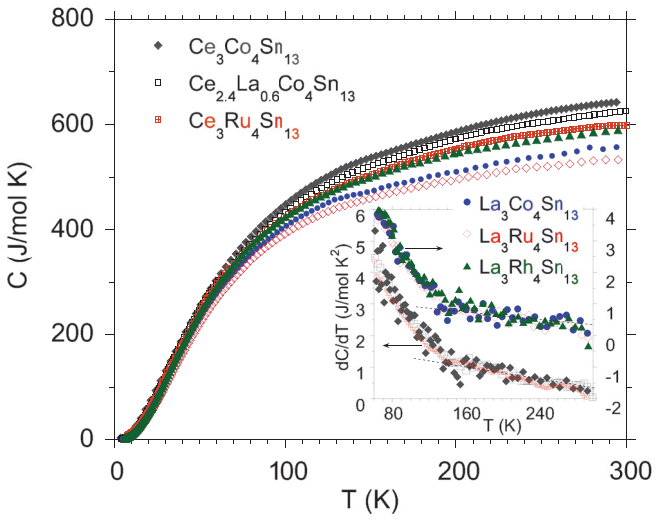

FIG. 12. (Color online) Specific heat of $La_3M_4Sn_{13}$, where M = Co, Ru, and Rh, and $Ce_3M_4Sn_{13}$ vs temperature. The inset displays derivative of C, $dC(T)/dT$. In all cases, the rapid change in the slope of $dC(T)/dT$ is visible at ∼160 K.

C with a change in the slope of $dC(T)/dT$ observed either for $Ce_3M_4Sn_{13}$ and their La counterparts at about 160 K. This $dC(T)/dT$ behavior signals the same nature of the transition occurring in all compounds reported on in this work. In addition to the XRD data (Figs. 1 and 2) and the results from Rietveld analysis in Table I, the change in the heat capacity at about 160 K is very likely due to the slight movement and distortion of the Sn2 atom from its initial position. (iii) Finally, the electrical resistivity of the $Ce_3M_4Sn_{13}$ shows a kink at about 160 K, evidently due to a structural change (see Refs. 2 and 3); the $\rho(T)$ data for $La_3Co_4Sn_{13}$ exhibits anomalous change near ∼140 K too, which provides evidence for the *nonmagnetic* character of this phase transition.

IV. CONCLUSSIONS

The recent density functional calculations[5,6] showed high charge density accumulation in $Ce_3M_4Sn_{13}$ between metal M and Sn2 atoms, which implies a strong covalent bonding interaction, while only weak bonding interactions exist between Sn1 and Sn2, Ce(La) and Sn2, as well as Ce(La) and metal M. It was also confirmed theoretically that the strong hybridization occurs between Co $3d$ and Sn2 $5p$ states near the Fermi level. Even a small change of a local symmetry, e.g., of the $M(Sn2)_6$ prisms generated by small deformation of the Sn_{12} icosahedra can lead to variation in the charge density of metal M and Ce ions. The principal purpose of this work was to investigate the electronic structure of Sn and determine the role of the on-site hybridization between the $4f$ electron and conduction electron states onto physical properties of $RE_3M_4Sn_{13}$ compounds. We present the Sn $4d$ XPS spectra measured at room temperature and at ∼130 K, i.e., below the subtle structural distortion observed at T_D. We have shown the complex structure of the $4d$ Sn XPS line, which is unusual, and interpreted this behavior as result of charge distribution around Sn2 atoms. The shape of the $4d$ Sn XPS line is also dependent on the temperature; its shape at 300 K differs from the line shape at $T = 130$ K. The effect can be attributed to the local distortion, which modifies the charge density accumulation in the vicinity of Sn atoms, and seems to be comparable in all investigated samples $Ce_3M_4Sn_{13}$ and $La_3M_4Sn_{13}$. Hybridization between the f-electron states and the conduction electron states is another reason of the variation in charge density distribution. The Δ_{cf} parameter of $Ce_3Co_4Sn_{13}$ is twice as large as it is in the remaining $RE_3M_4Sn_{13}$ compounds. For $Ce_3Co_4Sn_{13}$ the temperature dependence of the resistivity is quite different than for remaining compounds; it displays a metallic behavior above T_D, while below this temperature, the $\rho(T)$ is similar to that of $Ce_3Rh_4Sn_{13}$ and La-reference compounds.[3] We suggest that the stronger hybridization energy Δ in $Ce_3Co_4Sn_{13}$ is an additional contribution, which leads to the semimetal-metal transition at T_D in this metal, while the remaining $Ce_3M_4Sn_{13}$ and $La_3M_4Sn_{13}$ compounds exhibit metallic behavior above and below T_D.

ACKNOWLEDGMENTS

We thank the National Science Centre (NCN) for financial support, on the basis of Decision No. DEC-2012/07/B/ST3/03027.

[1] J. P. Remeika, G. P. Espinosa, A. S. Cooper, H. Barz, J. M. Rowel, D. B. McWhan, J. M. Vandenberg, D. E. Moncton, Z. Fizk, L. D. Woolf, H. C. Hamaker, M. B. Maple, G. Shirane, and W. Thomlinson, Solid State Commun. **34**, 923 (1980); J. L. Hodeau, M. Marezio, J. P. Remeika, and C. H. Chen, *ibid.* **42**, 97 (1982).

[2] E. L. Thomas, H.-O. Lee, A. N. Bonkston, S. MaQuilon, P. Klavins, M. Moldovan, D. P. Young, Z. Fisk, and J. Y. Chan, J. Solid State Chem. **179**, 1642 (2006).

[3] A. Ślebarski, B. D. White, M. Fijałkowski, J. Goraus, J. J. Hamlin, and M. B. Maple, Phys. Rev. B **86**, 205113 (2012).

[4] C. S. Lue, H. F. Liu, S.-L. Hsu, M. W. Chu, H. Y. Liao, and Y. K. Kuo, Phys. Rev. B **85**, 205120 (2012).

[5] M. Gamża, W. Schnelle, A. Ślebarski, U. Burkhardt, R. Gumeniuk, and H. Rosner, J. Phys.: Condens. Matter **20**, 395208 (2008).

[6] G. Zhong, X. Lei, and J. Mao, Phys. Rev. B **79**, 094424 (2009).

[7] K. Koepernik and H. Eschrig, Phys. Rev. B **59**, 1743 (1999); I. Opahle, K. Koepernik, and H. Eschrig, *ibid.* **60**, 14035 (1999); K. Koepernik, B. Velicky, R. Hayn, and H. Eschrig, *ibid.* **55**, 5717 (1997); H. Eschrig, K. Koepernik, and I. Chaplygin, J. Solid State Chem. **176**, 482 (2003).

[8] J. P. Perdew and Y. Wang, Phys. Rev. B **45**, 13244 (1992).

[9] J. J. Yeh and I. Lindau, At. Data Nucl. Data Tables **32**, 1 (1985).

[10] J. Rodriguez-Carvajal, Physica B **192**, 55 (1993).

[11] P. W. Anderson, Phys. Rev. **124**, 41 (1961).

[12] O. Gunnarsson and K. Schönhammer, Phys. Rev. B **28**, 4315 (1983); J. C. Fuggle, F. U. Hillebrecht, Z. Zolnierek, R. Lässer, Ch. Freiburg, O. Gunnarsson, and K. Schönhammer, *ibid.* **27**, 7330 (1983).

[13] S. Doniach and M. Šunjić, J. Phys. C **3**, 285 (1970).

[14] A. Ślebarski, T. Zawada, J. Spałek, and A. Jezierski, Phys. Rev. B **70**, 235112 (2004).

[15] Y. Baer and Ch. Zürcher, Phys. Rev. Lett. **39**, 956 (1977).

[16] Y. Baer, R. Hauger, Ch. Zürcher, M. Campagna, and G. K. Wertheim, Phys. Rev. B **18**, 4433 (1978).

[17] J. Dijkstra, E. A. Broekhuizen, C. F. van Bruggen, C. Haas, R. A. de Groot, and H. P. van der Meulen, Phys. Rev. B **40**, 12111 (1989).

[18] B. Lai, X. M. Ding, Z. L. Yuan, X. Zhou, L. S. Liao, S. K. Shang, S. Yuan, X. Y. Hou, E. D. Lu, P. S. Xu, and X. Y. Zhang, Appl. Surf. Sci. **157**, 35 (2000).

[19] R. S. Mulliken, J. Chem. Phys. **23**, 1833 (1955).

[20] L. E. Klintberg, S. K. Goh, P. L. Alireza, P. J. Saines, D. A. Tompsett, P. W. Logg, J. Yang, B. Chen, K. Yoshimura, and F. M. Grosche, Phys. Rev. Lett. **109**, 237008 (2012).

[21] A. H. Wilson, Proc. R. Soc. London A **167**, 580 (1938); also see N. F. Mott and H. Jones, *The Theory of the Properties of Metals and Alloys* (Oxford University Press, Oxford, 1950), p. 240.

[22] F. Canepa and S. Cirafici, J. Alloys Compd. **232**, 71 (1996).